# The influence of biofilms on the mobility of bare and capped zinc oxide nanoparticles in saturated sand and glass beads

# The influence of biofilms on the mobility of bare and capped zinc oxide nanoparticles in saturated sand and glass beads

H. Kurlanda-Witek[a], B.T. Ngwenya[b], I.B. Butler[b]

[a]*Mott MacDonald Polska Sp. z o.o., ul. Waliców 11, 00-851 Warsaw, Poland*

[b]*School of GeoSciences, University of Edinburgh, Kings Buildings, West Mains Rd, EH9 3JW Edinburgh, United Kingdom*

Email: hanna.kurlanda@yahoo.com

Tel. (04822) 649-4237

## Abstract

Biofilms are a common constituent of the subsurface and are known to influence contaminant transport; however only a few studies to date have addressed microbial controls on nanoparticle mobility in porous media. The impact of a 3-day *Pantoea agglomerans* biofilm on the mobility of zinc oxide (ZnO) nanoparticles was studied in column experiments containing sand and glass beads at near-neutral pH and constant ionic strength. Bare ZnO nanoparticles (bZnO-NPs) and ZnO nanoparticles capped with tri-aminopropyltriethoxysilane (cZnO-NPs) were used in the experiments. Breakthrough curves demonstrate that the biofilm particularly slowed nanoparticle migration of bZnO-NPs in glass bead columns and cZnO-NPs in sand columns. With the exception of bZnO-NPs in sand columns, biofilm-coated porous media retained more nanoparticles than controls without biofilm. The biofilm may bear an impact on the surface charge of the porous media, nullifying porous media-specific effects. Although viable cell counts (VCCs) decreased after the introduction of electrolyte and before nanoparticle transport experiments, SEM and CLSM imaging of porous media samples taken from columns after nanoparticle transport experiments, as well as total organic carbon (TOC) measurements reveal that biofilm was present in the columns throughout the experiments. Hence, it can be concluded

that even a thin amount of biofilm can hinder nanoparticle migration in small-scale porous media experiments. Moreover, nanoparticle mobility is dependent on the binding capacity of biofilms, rather than the type of porous media.

## 1. Introduction

The widespread production of nanoparticles by various industries and the associated concern that inadvertent release to the environment might impact ecosystem functioning has led to increase in research efforts to understand nanoparticle transport in porous media (Chowdhury et al., 2011; He et al., 2009). Zinc oxide (ZnO) nanoparticles are of particular concern as they are widely used in sunscreens and other personal care products (Newman et al., 2009). Nanoparticles may be introduced into the subsurface via precipitation, landfill waste, wastewater, or through the use of nanoparticle-bearing sludges in agriculture (Gajjar et al., 2009). Thus, nanoparticles migrate directly or indirectly into the biosphere, including into groundwater supplies, where the long-term effects of exposure have not yet been established (Dybowska et al., 2011; Li et al., 2011a).

Studies to date have shown that the transport of nanoparticles in porous media depends on a variety of factors, including the presence of capping agents (Petosa et al., 2012), ionic strength (Chowdhury et al, 2011), dissolved organic carbon (Ben-Moshe et al., 2010) and surface chemistry of the porous media (Kurlanda-Witek et al., 2014); however, the large surface area of porous media grains serves as an ideal environment for formation of microbial biofilms under favourable conditions (Kapellos et al., 2007). Biofilms consist of structured communities of one or more strains of microorganisms, bound together by gel-like extracellular polymeric substances (EPS), secreted by the microorganisms (Ross and Bickerton, 2002). They are frequent in the subsurface, where enhanced growth between porous media grains can lead to clogging of aquifer materials (Seifert and Engesgaard, 2012; Thullner et al., 2004; Yang et al., 2013). The abundance of microbial activity suggests that microbe-nanoparticle reactions are

likely to be fundamental in nanoparticle transport, and may even have applications in the treatment of nanoparticle-bearing wastewaters (Morrow et al., 2010).

Despite this knowledge, relatively few studies have investigated the impact of biofilms on nanoparticle transport. Consequently, our knowledge of the behaviour of nanoparticles under natural conditions found in the subsurface is limited. In a study on fullerene ($C_{60}$) nanoparticle transport in sand coated with an *Escherichia coli* (*E. coli*) biofilm, Tong et al. (2010) found that biofilm promoted higher nanoparticle deposition. Tripathi et al. (2012) demonstrated similar findings in transport experiments conducted with sulphate and carboxyl-modified latex nanoparticles and carboxyl-modified CdSe/ZnS quantum dots in sand columns with a *Pseudomonas aeruginosa* biofilm, as shown by larger attachment efficiencies and lower breakthrough curves. Jiang et al. (2013) stated that an *E. coli* biofilm growing on quartz sand retained ZnO nanoparticles irrespective of particle size and surface chemistry of the quartz sand grains. However, Lerner et al. (2012) found that a *Pseudomonas aeruginosa* biofilm had little influence on the transport and retention of iron nanoparticles in glass bead columns, and conversely, the modelled single collector contact efficiencies of nanoparticles were higher in sterile columns. The general status of these studies is that biofilm increases the affinity of nanoparticles to porous media, however there are exceptions, brought on by differences in ionic strength of the electrolyte, and by stabilisation of nanoparticles with polymers, which may promote steric repulsion between biofilm-coated porous media and nanoparticles (Xiao and Wiesner, 2013). However the effect of varying surface chemistry of the porous media on biofilm influenced nanoparticle mobility has not been studied. As shown in our previous study, the mineralogical composition and hence surface chemistry of the porous media causes fundamental differences in the transport behaviour of nanoparticles (Kurlanda-Witek et al., 2014).

The aim of this study was to develop a mechanistic understanding of the impact of biofilms on the transport on ZnO nanoparticles in saturated porous media, comparing glass beads with quartz sand, chosen because they have different surface charge characteristics under the simulated, near-neutral pH and low ionic strength conditions of the subsurface environment. We hypothesized that the presence of a biofilm could homogenize the surface chemistry of the porous media and hence nullify porous media specific effects. The important role of net-surface charge was investigated by also comparing bare and capped ZnO nanoparticles (bZnO-NPs and cZnO-NPs, respectively), the latter of which were capped with KH550 (tri-aminopropyltriethoxysilane).

## 2. Materials and methods

### 2.1 Porous media preparation and column packing

Two types of porous media were used for nanoparticle transport experiments; glass beads (0.5 mm in diameter), and quartz sand sieved to a diameter between 120 µm and 350 µm. They were chosen because despite similar chemical composition, they had different zeta potentials when measured under the conditions of the column experiments (5mM NaCl, pH ~8, Table 1). Both water and porous media were autoclaved and the porous media were dried under UV light in order to maintain sterility. Prior to autoclaving, sand and glass beads were washed three times in 6% hydrogen peroxide ($H_2O_2$) to remove any organic material, and then soaked in 10% nitric acid ($HNO_3$) overnight to remove any metals. The porous media were then washed in deionized water and made alkaline with 1 M sodium hydroxide (NaOH) to pH 7. All tubing and column parts used in the experiments were autoclaved and dried under UV light prior to use. Columns (12 cm working length and 1 cm diameter; Diba Omnifit) were packed with autoclaved 5 mM sodium chloride (NaCl) electrolyte and porous media. The columns were

packed in a Bio-Air microbiological safety cabinet (Aura B4 model) using the wet packing technique (Deshpande and Shonnard, 1999).

### 2.2 Preparation of nanoparticle solutions

bZnO-NP solution was purchased from Sigma Aldrich (100 ml of 50 w/t % solution in pure water, 30 nm average nanoparticle diameter). The stock solution was dispersed using an ultrasonic bath for 30 minutes. One ml of stock solution was diluted in deionized water to a concentration of 12.5 mg/ml and sonicated as above for 10 minutes. One ml of this solution was dispersed in 5 mM NaCl solution, made with autoclaved, deionized water to make up 1 l, and sonicated for a further 10 minutes. cZnO-NPs (20 nm average nanoparticle diameter), coated with 1 wt % KH550, a silane coupling agent, were purchased in powder form from US Research Nanomaterials Inc. Stock solutions were made by dissolving 0.5 g of nanoparticle powder in 1 l of 5 mM NaCl solution, and sonicated for 1 hour. A solution at a concentration of 12.5 mg/ml was made up with 5mM NaCl, then sonicated for a further 30 minutes. Both bZnO-NP and cZnO-NP solutions were analysed for average size of nanoparticles and zeta potential using dynamic light scattering (DLS) on a Zetasizer Nano ZS (Malvern Instruments Ltd.). Zeta potentials of crushed glass beads, crushed sand, *Pantoea agglomerans* culture, as well as a *P. agglomerans* biofilm grown on crushed beads and crushed sand, in 5 mM NaCl, pH = 8.0, were also established. Porous media was crushed to a powder using a mortar and pestle. Two ml of *P. agglomerans* culture was added to 5 g of crushed beads and 5 g of crushed sand one day prior to zeta potential measurements, and stirred on a rotary shaker at 30ºC overnight, to enable biofilm growth on the porous media grains. The supernatant, containing nutrient media, was decanted, and 2 ml of 5 mM NaCl was added to the samples. All sample suspensions were vortexed prior to measurement. Zeta potential measurements were measured in three runs of ten cycles each. Additionally, nanoparticle sizes were calculated from the Brus

equation, based on the UV-Visible absorbance spectra of nanoparticles in suspension (Brus, 1984) (see section 2 in Supporting Information, SI).

### 2.3 Column transport experiments

All experiments were performed in duplicate. The electrolyte was adjusted to pH 8 using 0.01 M NaOH, to prevent dissolution of zinc oxide nanoparticles (Jiang et al., 2012; Petosa et al., 2012). Several pore volumes of 5mM NaCl electrolyte were pumped into the columns using a peristaltic pump (Masterflex) at a flow rate of 0.46 ml/min (approximately 9 m/d). For biofilm columns, Nutrient Broth media (NM, 13 g/l) (No. 3, Fluka) was pumped into columns at a flow rate of 0.46 ml/min. After several pore volumes had been eluted, the columns were inoculated with 1ml of *Pantoea agglomerans*, an aerobic Gram negative bacteria commonly found in soil and water environments, that does not produce large amounts of EPS (Kapetas, 2012). *Pantoea agglomerans* was grown in liquid cultures (13 g/l NM in 100 ml) for a period of 24 hours. The aim was to cover the porous media grains with a thin layer of biofilm, without facilitating physical bioclogging, and thus the creation of preferential flow paths. The columns were left for 24 h to allow attachment of the bacteria onto the porous media. Afterwards, NM was pumped into the columns continuously at a flow rate of 0.5 ml/min for a period of 3 days. Outflow and viable cell counts were measured daily. Approximately 12 h before nanoparticle solutions were pumped into the columns, 5 mM NaCl electrolyte was pumped into the columns at a flow rate of 0.46 ml/min in order to flush out all traces of NM, which could enhance nanoparticle aggregation due to salt content and the presence of organic material (Ben-Moshe et al., 2010). Viable cell counts in the effluent were also determined after 12 h of addition of electrolyte and before nanoparticle transport experiments in order to verify that bacteria were still present in the columns after the addition of electrolyte. Sterile control column experiments were carried out by pumping several pore volumes of electrolyte before pumping in nanoparticle solution. For both control and biofilm columns, 3 pore volumes of nanoparticle

solution were pumped into the column at a constant flow rate, followed by 5 pore volumes of electrolyte. Nanoparticle concentration in the samples was measured as dissolved Zn using ICP-OES. Concentrated $HNO_3$ was added to measured samples to a concentration of 2% (Yang et al., 2013). Acidified samples were analyzed using a Perkin Elmer Optima 5300 DV ICP-OES, with analytical uncertainties determined using a certified multi-element standard (CertiPUR ICP multi-element (M6) standard for ICP-MS, Merck). Nanoparticle input solutions were collected before entering the columns, throughout the duration of the nanoparticle transport experiments (at the beginning of pore volumes 1, 2 and 3). Concentrations measured in column outflow were normalized to averaged values in the input solution in order to calculate the breakthrough curves ($C/C_0$).

After the transport experiments, columns were dismantled and the porous media mass was divided into 5 sections. 2.5 ml of 2% $HNO_3$ was added to 0.5 g of glass beads or sand from each column section and stirred overnight to detach ZnO from the beads. In a previous study, mass balance calculations demonstrated that the majority of nanoparticles remained attached to the porous media grains (Kurlanda-Witek et al., 2014). Extractions were performed in duplicate. After 24 h, the acidified samples were centrifuged at 24149 × g, for 20 min, at 4°C, and filtered through 0.22 µm filters for ICP-OES analysis (Yang et al., 2013). The remaining porous media samples from biofilm columns were used for Total Organic Carbon (TOC) determination as a proxy for biofilm biomass distribution (see section 3 in SI).

### 2.4 Determination of viable cell counts

Viable cell counts were conducted in order to observe biofilm viability throughout the duration of the experiment. Cell counts of inoculated columns were determined by plating serial dilutions of effluent. One ml of effluent was diluted between $10^{-1}$ and $10^{-6}$ times using sterile, deionized water. Each dilution was gently mixed using a vortex (Vortex Genie, Scientific Industries). Ten µl of each dilution was pipetted and spread onto plates with Nutrient

Agar (Fluka) and incubated in an oven for 24 hours, after which colonies were counted (Brock and Madigan, 1991).

### 2.5 Confocal laser scanning microscopy (CLSM) and scanning electron microscopy (SEM)

Confocal laser scanning microscopy (CLSM) was used to observe the extent of biofilm growth on porous media after termination of experiments. Biofilm samples grown on sand were washed with phosphate buffered saline (PBS) and stained with 4',6-diamidino-2-phenylindole (DAPI) stain at a concentration of 300 µg/ml, made from 10 mg/ml stock solution (Biotium), using PBS as diluent. Samples were fixed onto glass slides using SlowFade Gold Antifade Reagent (Invitrogen), and air-dried. Glass beads were too big to mount on glass slides, therefore 0.5 g of beads were vortexed with PBS and stained with DAPI stain, and a drop was placed on a glass slide and left to air-dry. Once dried, the samples were covered with glass cover slips and fixed with nail varnish. Samples were viewed using a Leica SP5 Confocal Laser Microscope. Stacks of images were processed to 3D images using ImageJ software. Scanning electron microscopy (SEM) images were taken of porous media from the top and bottom sections of each column. Porous media was transferred with a spatula onto 1 cm diameter SEM stubs, and gold sputtered using a BAL-TEC SCD 050 Sputter Coater. Samples were viewed with a Philips XL30CP scanning electron microscope in secondary electron imaging mode. Surfaces of porous media were visualized using a Nikon SMZ800 stereo microscope with attached Nikon Coolpix 995 digital camera.

# 3. Results

## 3.1 Nanoparticle size range and zeta potentials of nanoparticles and porous media

Measurements by DLS of bZnO-NPs in suspension determined an average diameter of 72 nm, while cZnO-NPs were an average 45.1 nm in diameter. Because DLS is a particle size measurement tool based on scattering light by particles in suspension, the results are skewed in favour of larger, aggregated nanoparticles (Quevedo and Tufenkji, 2012), implying that the majority of nanoparticles were likely to be smaller than the size measured. The UV-Vis spectra of nanoparticle suspensions was interpreted using the Brus equation (Brus, 1984) as an alternative to DLS to estimate nanoparticle sizes, yielding sizes of 6.6 nm and 14.6 nm (± 2 nm) for bZnO-NPs and cZnO-NPs, respectively (see section 2 in Supporting Information).

Table 1 presents results for zeta potentials of porous media, nanoparticles and bacteria used in the experiments. Mean zeta potentials for nanoparticle suspensions were +21 ± 2.74 mV and +1.45 ± 1.6 mV for bZnO-NPs and cZnO-NPs, respectively. Positive zeta potentials for bZnO-NPs were also reported by Ben-Moshe et al. (2010), Petosa et al. (2012), and Zhou and Keller (2010). Capping ZnO nanoparticles with polymers can change the zeta potential to negative values at neutral pH (Kanel and Al-Abed, 2011; Petosa et al., 2012); however, KH550 has a circumneutral surface charge at near neutral pH, due to the presence of both negatively charged silanol groups and positively charged amino groups (Metwalli et al., 2006). Zeta potential results for cZnO-NPs in 5mM NaCl varied between -4.9 mV and +14.78 mV. Chen et al. (2001) found that the zeta potential of quartz sand modified with aminosilane was equal to approximately 0 mV. Glass beads (-35.2 ± 5.89 mV) and sand (-53.9 ± 4.03 mV) were negatively charged in 5 mM NaCl and pH=8, which was expected, as the points of zero charge (PZC) for glass and sand are approximately pH=2 for both materials (Kosmulski, 2009). *P. agglomerans* culture was also negatively charged, as bacterial cell walls are negatively charged at most

environmental pHs, which leads to their affinity to metals (Kapetas et al., 2012). The addition of biofilm increases the net negative zeta potential for glass beads to a value close to that of quartz sand but largely leaves that of quartz sand unaffected; hence the presence of biofilm leads to identical zeta potentials. The different effect on zeta potential may be due to the sparse cover of biofilm on sand. This was also found by Lerner et al. (2012) on glass beads. In fact, the uneven biofilm growth on glass beads have led Lerner et al. to believe that the zeta potential is incorrect.

### 3.2 Viable cell counts (VCC)

The number of viable cells in column effluent was evaluated as an estimate of biofilm viability. The limitation of this method is that the amount of viable cells in the effluent may not provide information on the actual stability of the biofilm, or what proportion of the biofilm may actively uptake nanoparticles. VCCs were calculated from the four experiments in which biofilm growth took place (each experiment was performed in duplicate). It was anticipated that there could be differences in the amount of viable cells between glass bead and sand columns, with respect to greater surface area of sand grains. Figure 1 shows the average number of VCCs from four experiments (with duplicates): columns from bZnO-NP experiments packed with sand and glass beads, and columns from cZnO-NP experiments packed with sand and glass beads. The VCCs were carried out daily prior to nanoparticle transport, and were additionally carried out on Day 4, directly before the nanoparticle transport experiments. VCCs increased over a period of three days of biofilm growth, to an average of $9.6\times10^4$ cells/ml. After approximately 12 hours of 5 mM NaCl electrolyte solution flowing through the columns, cell counts dropped to an average of $2.6\times10^4$ cells/ml, signifying that the electrolyte either killed cells or stripped biofilm from the collector grains. This was the case in all of the experiments, except for experiment 2 of the sand columns (cZnO-NP transport experiment) (Figure 1). VCC values are twice as high in sand columns, compared to glass bead columns ($p$= 0.08).

### 3.3 Breakthrough curves

Figure 2 shows breakthrough curves for bare (2a and 2b) and capped (2c and 2d) nanoparticles, each comparing controls with biofilm coated porous media. Outflow samples were collected at 1-minute intervals with the intention of measuring the breakthrough curve using UV-Visible absorption spectroscopy. However, these measurements yielded erratic results, possibly due to aggregation of the nanoparticles after collection. Consequently, samples were analysed using ICP-OES. Hence, samples from duplicate experiments were batched together to yield sufficient volume, so that the breakthrough curves presented in Figure 2a are a moving average of the results.

More bZnO-NP breakthrough was observed in control bead columns relative to sand control columns, where nanoparticles were close to detection limit. Introduction of biofilm resulted in identical breakthrough curves for bead and sand columns, being identical to those of control sand columns. This observation is consistent with the similar surface charge characteristics measured for biofilm coated beads and sands. However, as the breakthrough curves of bZnO-NP transport are the same in sand columns, it is difficult to determine the actual effects of biofilm on these nanoparticles.

By contrast, significant differences were observed in the transport of cZnO-NPs between bead control and sand control columns (Figures 2c and 2d). In glass bead columns, the breakthrough curve of cZnO-NPs from columns with biofilm growth is similar in shape to the control columns (Figure 2c), which are in turn much lower than those in the sand control column. The reason for this could be uneven distribution of biofilms on the surface of the glass beads, which is the nature of biofilm growth and not a feature of the collector grain (see section 4.1). In the case of sand control columns, the breakthrough curves of cZnO-NPs reached a plateau, but the nanoparticle breakthroughs were eluted after the same pore volumes as for glass beads. A small tailing effect was also observed. By contrast, nanoparticles were not

detected in the biofilm colonised sand columns. In general, cZnO-NPs were more mobile than bZnO-NPs, particularly in sand (Figure 2d).

### 3.4 Retention profiles

Retention profiles determined by extracting nanoparticles from the columns after flow experiments are shown in Figure 3. For bZnO-NPs (Figures 3a and 3b), there was only a statistically significant difference in retention at the column inlets of glass bead columns (Figure 3a), where columns with and without biofilm retained an average of 67.6 ± 4.9 µg/g vs 36.3 ± 8.5 µg/g nanoparticles ($p$ = 0.02). Sand columns with and without biofilms retained 45 ± 4 µg/g vs. 97 ± 19.8 µg/g of nanoparticles ($p$ = 0.23) (Figure 3b). For cZnO-NPs, nanoparticle retention was marginally higher in the biofilm columns of glass beads, except at the inlet, where retention was equal between biofilm and control columns (Figure 3c), whereas in sand columns, nanoparticle retention values were generally lower for biofilm-coated sand, yet higher at the inlet (Figure 3d). In general, retention profiles of cZnO-NPs were smaller than for bZnO-NPs, signifying higher elution rates for the capped nanoparticles.

### 3.5 Calculation of single collector contact efficiency and attachment efficiency

Colloid filtration theory (CFT) (Yao et al., 1971) was used to quantitatively analyse the deposition behaviour of ZnO nanoparticles in both saturated sand and glass beads, with and without attached biofilm, based on nanoparticle breakthrough curves in column experiments.

Attachment efficiencies were calculated for $C/C_0$ values determined at approximately 1.5-2 pore volumes of the experiments to evaluate maximum attachment efficiencies for the clean-bed stage of ZnO nanoparticle attachment (Petosa et al., 2012). Hamaker constants for porous media, bacteria, and water were taken from Israelachvili (1992), whereas the Hamaker constant for ZnO nanoparticles was taken from Bergstrom (1997). The equations and parameters are

presented in section 4 of SI. The results of attachment efficiencies and single collector contact efficiencies for both bZnO-NPs and cZnO-NPs are presented in Tables 2 and 3, respectively.

The presence of biofilm did not significantly change the single collector contact efficiencies for bZnO-NPs in either glass beads or sand. This is due to the fact that the only difference between the calculations for coated and uncoated porous media in the Tufenkji-Elimelech equation is the change in Hamaker constant, which is very small (Lerner et al., 2012). bZnO-NPs had considerably higher attachment efficiencies to glass beads than to sand, which is inconsistent with our breakthrough curves and retention profiles of transport experiments in glass beads and sand columns, as elution of nanoparticles, albeit limited, occurred in glass bead control columns (Figures 2a and 2c). Biofilm almost doubled the attachment efficiency of glass beads ($2.53 \pm 0.0018$ for biofilm and $1.35 \pm 0.027$ for the control), whereas attachment efficiencies of sand were very similar with and without biofilm ($0.71 \pm 0.077$ and $0.79 \pm 0.006$ for the biofilm and control column, respectively), which agrees with breakthrough curves in that biofilm inhibited nanoparticle transport in glass bead columns and not in sand columns. $\alpha$ exceeded unity, signifying that more particles aggregate on the collector than are able to strike the collector (Kurlanda-Witek et al., 2014).

The overall attachment efficiencies for cZnO-NPs were lower than for bZnO-NPs and the results for the T-E correlation equation are in broad agreement with experimental data. Specifically, the attachment coefficient for the control sand columns was one order of magnitude lower than for control glass bead columns. This is correlated with breakthrough curves, where cZnO-NPs showed highest elution from control sand columns (Figure 2d). The addition of biofilm to sand columns greatly reduced nanoparticle elution, hence nanoparticle attachment to biofilms was higher ($\alpha = 0.22$). Moreover, nanoparticle attachment to glass beads with and without biofilm was comparable, which was also reflected by the respective breakthrough curves for glass bead columns (Figure 2c). Single collector contact efficiencies

for cZnO-NPs were higher for sand columns, indicating a higher predicted retention of nanoparticles; however, the total differences in retention between glass bead and sand columns were not substantial.

## 4. Discussion

### 4.1 Biofilm growth in columns

A primary objective was to obtain optimum biofilm growth levels, sufficient to observe an impact on nanoparticle transport. A longer period of biofilm growth could lead to clogging of the porous media, which would result in channelling of the fluid (Ozis et al., 2007). In the literature, biofilm growth in column experiments varies between 24 hours and 5 days (Lerner et al., 2012; Tripathi et al., 2012). For *Pantoea agglomerans* used in our experiments, 3 days may not have been sufficient for adequate growth, which is illustrated by almost all VCC measurements, carried out as an estimate of biofilm growth; however, SEM and CLSM imaging, as well as TOC, carried out at the end of the experiments, after over 18 hours of electrolyte flow and exposure to nanoparticles, demonstrated that biofilms still remained in the columns, even though a minimal number of viable cells was eluted from the columns (Figure 1). Figures 4a and 4b show that colonies of cells were attached to the sand grains. Moreover, Figure 4a suggests that the biofilm became thin and patchy, retreating into grain crevices. Cells were not visible on the exposed surfaces of the sand grains in the studied samples. However, the CLSM images (Figures 5 and 6) show that cells were attached to the overall surface of the porous media grain, with some local differences in cell concentration, which is particularly evident in the CLSM image of a sand grain, as the whole grain was visualized in situ. This uneven growth was also observed by Lerner et al. (2012), in a study of a *Pseudomonas aeruginosa* biofilm grown on glass beads, and by Xiao and Wiesner (2013) in Gram positive and Gram negative bacteria biofilms on glass beads. TOC measurements (Figure S2) show a

significant error between sample duplicates, which further stresses local differences in biofilm growth in porous media. Hence, it is frequently observed that biofilms are troublesome to produce repeatedly, even in replicate experiments (Lewandowski et al., 2004).

### 4.2 Mobility of bZnO-NPs in clean porous media

Control columns with both glass beads and sand show that bZnO-NPs had limited mobility. Nanoparticle mobility in glass bead columns was slightly higher than in sand columns, which can be associated with larger and rounder grains (He et al., 2009). However, bZnO-NPs are known to generally possess low mobility (Petosa et al., 2012). Ben-Moshe et al. (2010) confirmed that ZnO nanoparticles showed the lowest mobility in a comparison with three other metal oxide nanoparticles. This is due to the fact that ZnO has a positive zeta potential (+21 mV in our experiments) and binds to negatively charged glass bead or sand walls at near-neutral pH (zeta potentials of -35.17 mV and -53.94 mV in 5 mM NaCl, respectively). Figures 3a and 3b demonstrate that a significant amount of nanoparticles was retained in the columns, particularly close to the column inlet. This occurrence was also observed by Jiang et al. (2012) in their study on ZnO nanoparticle transport in sand columns, despite the fact that the nanoparticles used in their study were negatively charged under all conditions, and so were predicted to be repelled by the negatively-charged sand grains. The opposite zeta potentials of nanoparticles and collector grains in our experiments resulted in strong attractive forces, and subsequently favourable conditions for attachment (Kuhnen et al., 2000). This may have led to nanoparticle aggregation on entering the column, by filling binding sites on porous media surfaces (Chowdhury et al., 2011; Jiang et al., 2012). It should be noted that, as the bZnO-NPs possessed positive zeta potentials, aggregation of nanoparticles in solution was unlikely.

### 4.3 Mobility of cZnO-NPs in clean porous media

cZnO-NPs were generally more mobile than bZnO-NPs in negatively-charged porous media (Figures 2c and 2d vs. Figures 2a and 2b, respectively). KH550, used to coat the nanoparticles, changed the zeta potential of ZnO nanoparticles to a small positive or neutral value in 5 mM electrolyte. While this may infer instability of the suspension, as high absolute values of zeta potential cause nanoparticles to repel one another, breakthrough curves from our experiments suggest that the suspensions were stable, as nanoparticle instability would be demonstrated by a high tendency to aggregate (Sato et al., 2011). Moreover, solving the Brus equation for cZnO-NP size based on the UV-Visible absorbance spectrum implies that the actual nanoparticle size was 14.6 nm, as opposed to 45.1 nm, measured by DLS, which could be a measurement of aggregate size. The increased migration of cZnO-NPs in sand columns compared to glass bead columns was contrary to surface potential measurements, since sand grains had a more negative surface charge than glass beads; hence, the slightly positively-charged nanoparticles would be expected to bind more strongly to sand. It may be that the zeta potential for glass beads contains errors. Lerner et al. (2012) state that the zeta potential of crushed glass beads in 1 mM NaCl was -67.03 mV, which is nearly twice as negative as our result for crushed glass bead suspensions (-35.2 (± 5.89) mV in 5 mM NaCl). This could be attributed to surface charge heterogeneity of the glass beads. Nanoscale surface charge heterogeneity of collector grains is known to play a key role in the deposition of nanoparticles, and even minor changes in surface charge result in increased nanoparticle attachment (Torkzaban et al., 2010). The differences in migration between the two materials cannot be attributed to greater surface roughness for glass beads than for sand since surface roughness parameters in our experiments ruled out this phenomenon, as

roughness of sand grains was found to be higher than of glass beads, and both materials possessed low overall surface roughness parameters (Kurlanda-Witek et al., 2014).

Furthermore, it is also possible that differences in nanoparticle surface charge caused quicker elution of cZnO-NPs through sand columns. More positively charged nanoparticles in the nanoparticle suspension saturated binding sites on sand columns, leaving the less positively charged nanoparticles to flow through the column. Deposited nanoparticles will neutralize the overall charge and eventually break through (Wang et al., 2012).

### 4.4 Influence of biofilms on nanoparticle transport

Coating porous media surfaces with biofilm will further impede nanoparticle transport due to increased negative charge imparted by biofilm. In this pH range, EPS becomes negatively charged due to deprotonation of phosphate and carboxyl groups (Tourney et al., 2009). Indeed, in our experiments, the zeta potential of *Pantoea agglomerans* in 5 mM NaCl was determined to be -20.6 mV. Lower mobility is clearly evident in bZnO-NP transport in glass bead columns and cZnO-NP transport in sand columns, where breakthrough curves were lower and retention profiles show that more nanoparticles accumulated in columns with biofilms. For cZnO-NPs, lower mobility in inoculated sand columns compared to that of glass bead columns may be explained by a higher amount of viable cells in the sand columns, as demonstrated in Figure 1, and hence a higher nanoparticle deposition rate. Lower breakthrough curves were also observed by Tong et al. (2010) with fullerene ($C_{60}$) nanoparticle transport in sand columns with an *E. coli* biofilm, by Tripathi et al. (2012) with sulfonated polystyrene latex bead transport in sand columns, to which a *Pseudomonas aeruginosa* biofilm was introduced, by Li et al. (2013) with several nanoparticles in biofilm coated sand filters, as well as by Jiang et al. (2013) in ZnO nanoparticle transport in sand columns with an *E. coli* biofilm. All nanoparticles were negatively charged. This suggests that retention of nanoparticles by biofilms in porous media occurs regardless of bacterial strain or type of nanoparticle used; however, differences in the

breakthrough curves of bZnO-NPs in sand columns and cZnO-NPs in glass bead columns between transport experiments with and without biofilm are not particularly noticeable (Figure 2). An analogous situation was observed by Lerner et al. (2012) in columns with biofilm-coated and uncoated glass beads. Zerovalent iron nanoparticles capped with polyacrylic acid were used in the transport experiments, and NaCl electrolyte ionic strength was 1 mM. A higher retention rate of nanoparticles was observed in higher ionic strength electrolyte of 25 mM, an effect also demonstrated by Tong et al. (2010). This was explained by lower compression of the electrical double layer (EDL) of nanoparticles at low ionic strength, resulting in increased electrostatic repulsion between negatively charged polymer-coated nZVI and the negatively charged biofilm (Lerner et al., 2012). As the ionic strength remained constant in all of our experiments, another explanation for lack of biofilm impact on nanoparticle breakthroughs in some biofilm columns is that biofilm growth levels were higher in sand columns for cZnO-NP transport experiments, although all biofilms were grown under identical conditions. As was noted by Peulen and Wilkinson (2011), no two biofilms are the same. Some studies claim that short-term starvation of a biofilm increases cell attachment (Cunningham et al., 2007). Conversely, Walczak et al. (2012) found that cell mobility increased with an increase in pH and a decrease in ionic strength, as well as when the biofilm was additionally starved for 4-25 hours. This could be the scenario observed in our experiments, as switching from NM to electrolyte resulted in an increase in pH (from 7 to 8) and a decrease in ionic strength (NM contains a high salt concentration). However, in experiments conducted by Walczak et al. (2012) the cell culture was injected into sand-packed columns for only 60 minutes, which could be insufficient for cell adhesion to sand grains. Yang et al. (2013) demonstrated that biofilms grown in sand columns, subjected to minimal nutrient medium and high levels of exposure to dissolved zinc for one week still maintained good cell viability. SEM and CLSM images of biofilms from our experiments (Figures 4-6), which were taken after introduction of

nanoparticles, show that cells were still attached to sand grains, yet their mobility and/or viability could have been reduced. As demonstrated in cZnO-NP transport in sand, even a thin and patchy biofilm can impact nanoparticle transport (Figure 2d). TOC results also confirm that biomass was still present in the columns after termination of the experiments (Figure S2).

In previous studies, most transport experiments in biofilm-coated porous media were conducted with negatively-charged nanoparticles, in order to observe nanoparticle transport under unfavourable attachment conditions, i.e. repulsive interactions between negatively charged nanoparticles and negatively charged bacteria (Jiang et al., 2013; Lerner et al., 2012; Tong et al., 2010; Tripathi et al., 2012; Xiao and Wiesner, 2013). Studies of capped nanoparticles have also been conducted on batch tests of bacteria in order to explain the mechanisms of nanoparticle attachment and accumulation in bacterial cells. Dror-Ehre et al. (2010) grew *Pseudomonas aeruginosa* biofilms in microtiter plates, subjecting them to very high doses (10-180 µg/ml) of citrate-capped silver nanoparticles. The bacteria developed survival strategies by pushing the silver nanoparticles to the periphery of the cells. Stojak et al. (2011) studied the interactions of different-sized gold nanoparticles capped with citrate, with a *Legionella pneumophila* biofilm. The concentration of nanoparticles in suspension was very low; 0.7 µg/l, and yet nanoparticle absorption and aggregation was visible both on the inside and outside of the cells. This was, however, influenced by the size of the nanoparticles, as 50 nm nanoparticles were found not to interfere with biofilm morphology, compared to 4 and 18 nm-sized nanoparticles (Stojak et al, 2011). Habimana et al. (2011) reported that the diffusion of anionic carboxylate-modified fluorescent polystyrene nanoparticles depends on the cell wall hydrophobicity of *Lactococcus lactis* biofilms, which was also found by Xiao and Wiesner (2013), where hydrophobic biofilms retained most nanoparticles. These findings indicate that, despite the negative zeta potentials of capped nanoparticles, they are still prone to aggregation and diffusion into biofilms. In natural conditions, the production of EPS in biofilms triggered

by nanoparticle presence promotes embedding of the nanoparticles in the EPS matrix, leading to aggregation (Benzerara et al., 2011). This is most likely a survival mechanism for biofilm bacteria (Joshi et al., 2012). The favourable interaction of nanoparticles to EPS was also demonstrated in experiments with silica and hematite nanoparticles (Ikuma et al., 2014), as well as in experiments with metal nanoparticles in natural freshwater biofilms, where nanoparticle stabilization occurred regardless of external factors, such as pH (Kroll et al., 2014). It can be concluded that nanoparticles, irrespective of type and surface charge can bind to the extracellular matrix of biofilms, which was also observed in our experiments on a small scale, demonstrated by the enhanced binding of nanoparticles in biofilm columns at the column inlet.

## 5. Conclusions

The transport and retention of bare and capped ZnO nanoparticles in biofilm-coated glass beads and sand, at near-neutral pH and groundwater salinity, was studied. The mobility of both bZnO-NPs and cZnO-NPs was generally low with and without biofilms, as conditions for attachment were favourable. The effects of further decreased nanoparticle mobility in biofilms grown on porous media were primarily dependent on the extent of biofilm growth and subsequent nanoparticle binding capacity by bacteria and EPS, rather than the type of porous media used. This has positive environmental implications, as biofilms could be used as a potential remediation strategy against the migration of nanoparticles in heterogeneous aquifers. Further work on the impact of biofilms on nanoparticle transport in porous media is necessary, particularly using naturally-occurring mixed-culture biofilms and heterogeneous porous media.

| **Material** | **Zeta potential (mV) in 5 mM NaCl** |
|---|---|

| | |
|---|---|
| Bare ZnO nanoparticles | +21 (±2.74) |
| Capped ZnO nanoparticles | +1.45 (±1.57) |
| Crushed glass beads | -35.2 (±5.89) |
| Crushed sand | -53.9 (±4.04) |
| *Pantoea agglomerans* culture | -20.6 (±2.38) |
| Crushed glass beads + *P. agglomerans* | -52.1 (±2.33) |
| Crushed sand + *P. agglomerans* | -49.5 (±3.62) |

Table 1. Zeta potentials and standard error for nanoparticles, porous media, and bacteria used in transport experiments.

| **Parameter** | **Glass beads control** | **Sand control** | **Glass beads with biofilm** | **Sand with biofilm** |
|---|---|---|---|---|
| $\alpha$ | 1.35 ± 0.027 | 0.79 ± 0.006 | 2.53 ± 0.0018 | 0.71 ± 0.077 |
| $\eta_0 \times 10^{-3}$ | 8.2 | 14.3 | 7.4 | 13.6 |

Table 2. bZnO-NP attachment efficiencies with standard error and single collector contact efficiencies for glass beads and sand, with and without attached biofilm.

| **Parameter** | **Glass beads control** | **Sand control** | **Glass beads with biofilm** | **Sand with biofilm** |
|---|---|---|---|---|
| $\alpha$ | 0.78 ± 0.028 | 0.072 ± 0.0019 | 0.85 ± 0.035 | 0.22 ± 0.008 |
| $\eta_0 \times 10^{-3}$ | 11.8 | 20.7 | 10.8 | 17.7 |

Table 3. cZnO-NP attachment efficiencies with standard error and single collector contact efficiencies for glass beads and sand, with and without attached biofilm.

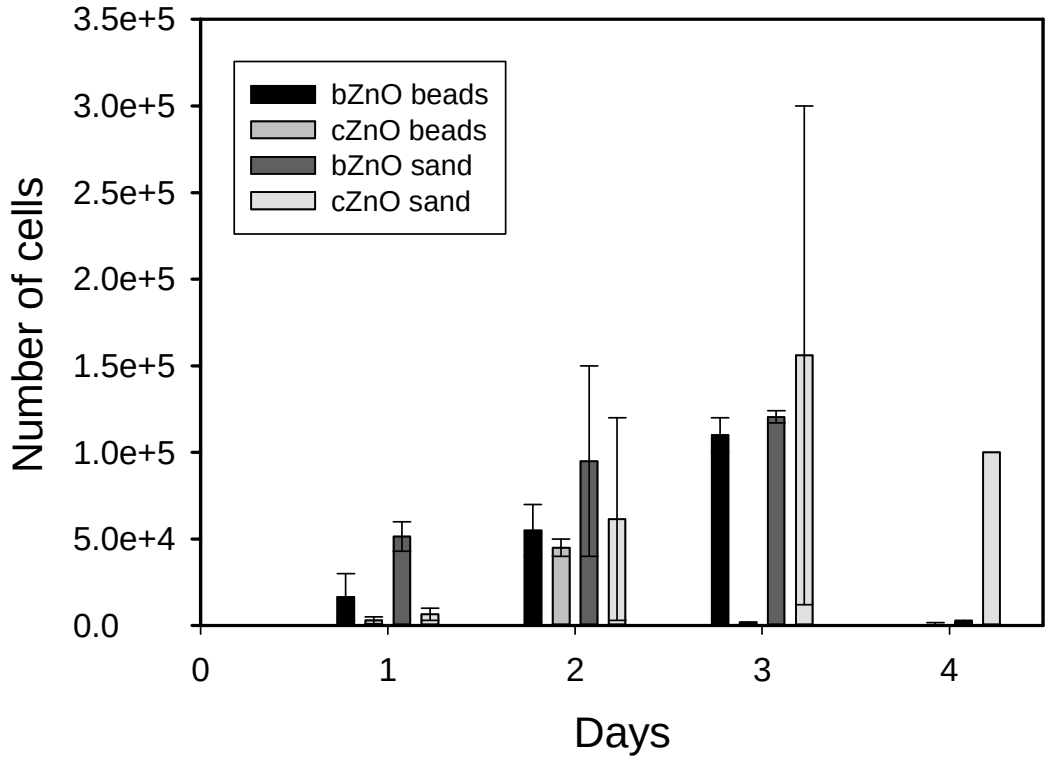


Figure 1. Average numbers of viable cells measured from outflow samples of duplicate sand and glass bead column experiments throughout the duration of biofilm growth. Transport experiments with either bZnO-NPs or cZnO-NPs were carried out after biofilm growth in porous media. Samples on Day 4 were taken after 12 hours of column flushing with electrolyte, directly before nanoparticle transport measurements. Error bars represent standard error between duplicate experiments.

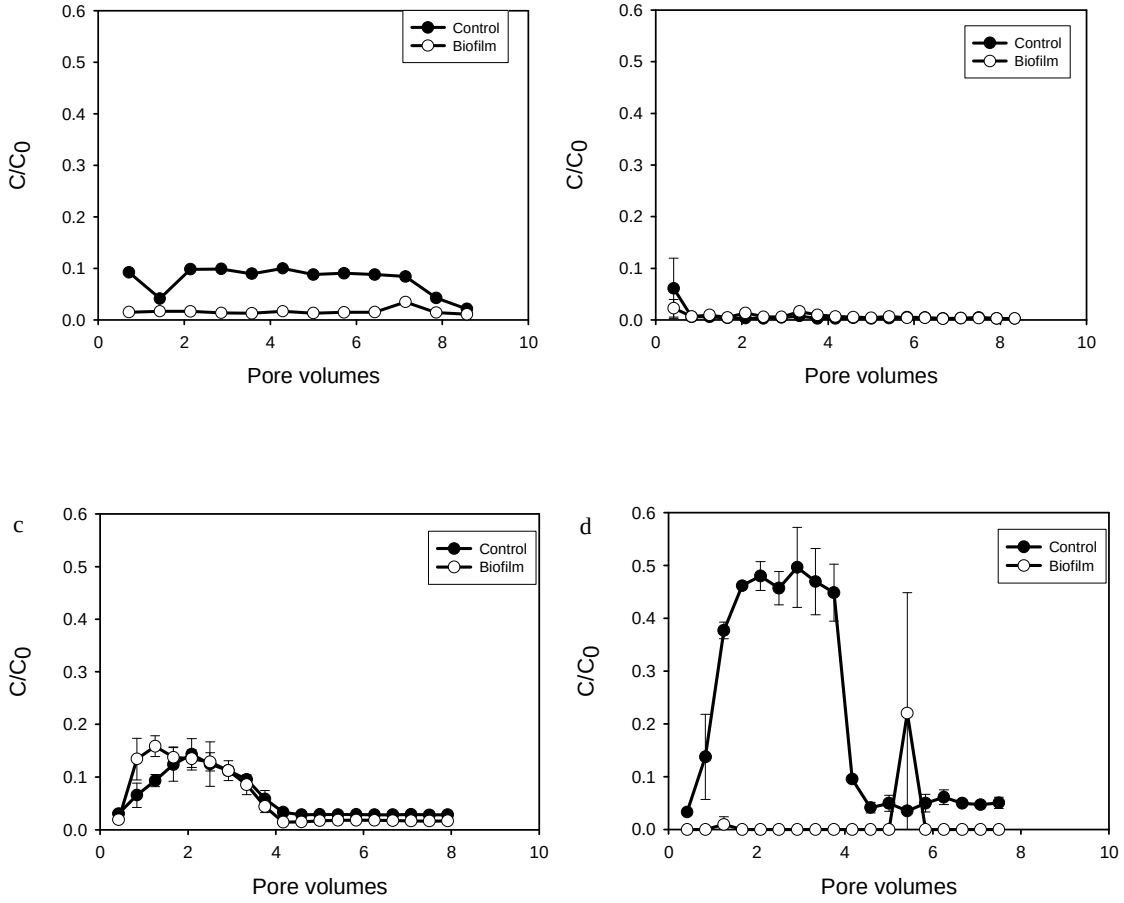


Figure 2. Breakthrough curves of a) bare ZnO nanoparticles (bZnO-NPs) in glass bead columns, b) bZnO-NPs in sand columns, c) capped ZnO nanoparticles (cZnO-NPs) in glass bead columns, and d) cZnO-NPs in sand columns, with and without biofilm. For glass bead columns, mobility of bZnO-NPs is lower in columns with biofilms; however bZnO-NP mobility is very low in sand columns with and without biofilms. Breakthrough curves in cZnO-NP columns packed with glass beads suggest that biofilms have no measurable impact on nanoparticle mobility, whereas biofilm growth impedes cZnO-NP transport in sand. Error bars represent standard error between duplicate experiments.

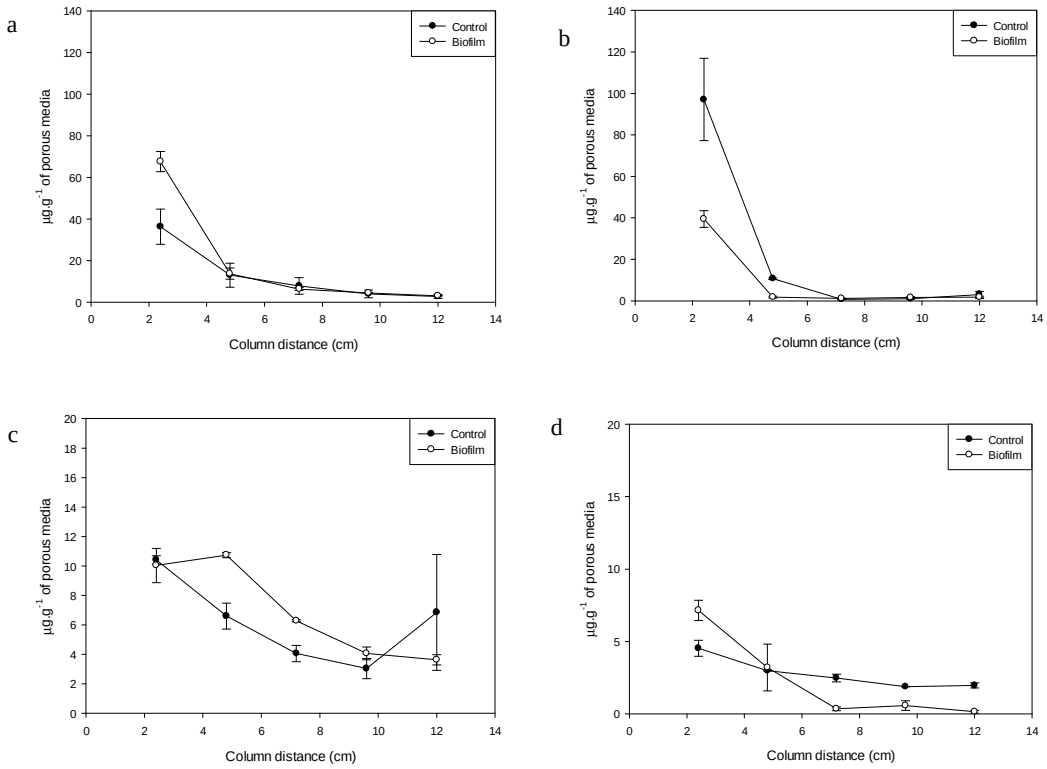


Figure 3. Retention profiles of bZnO-NPs in a) glass bead columns, b) sand columns, and cZnO-NPs in c) glass bead columns and d) sand columns, with and without biofilm. With the exception of bZnO-NP retention in sand columns, retention is greatest at the column inlets. Error bars represent standard error between duplicate samples.

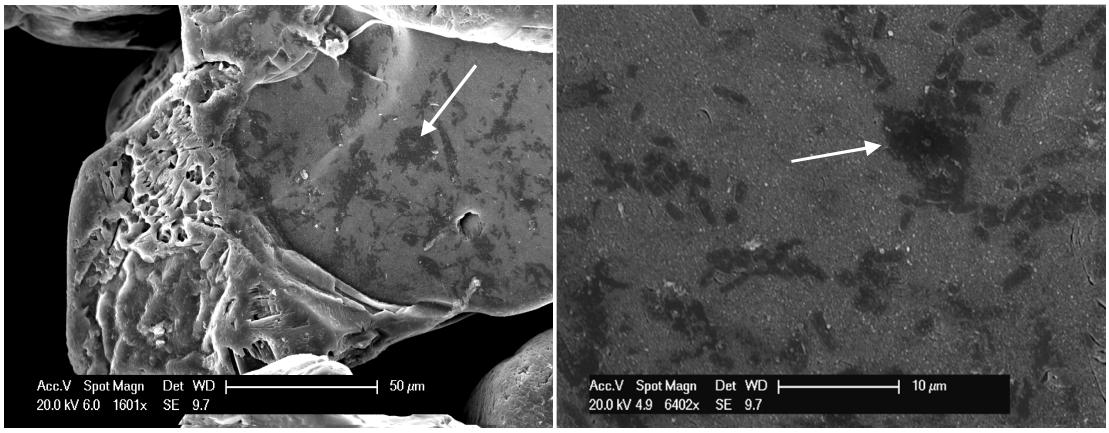


Figure 4. SEM images of *Pantoea agglomerans* cells adhering to a sand grain from the column inlet after a nanoparticle transport experiment; a) 50 µm resolution, b) 10 µm resolution. Larger colonies are marked by white arrows. These images demonstrate that bacterial colonies survive several hours of proximity to 12.5 ppm ZnO nanoparticle solution, probably by retreating to crevices of sand grains.

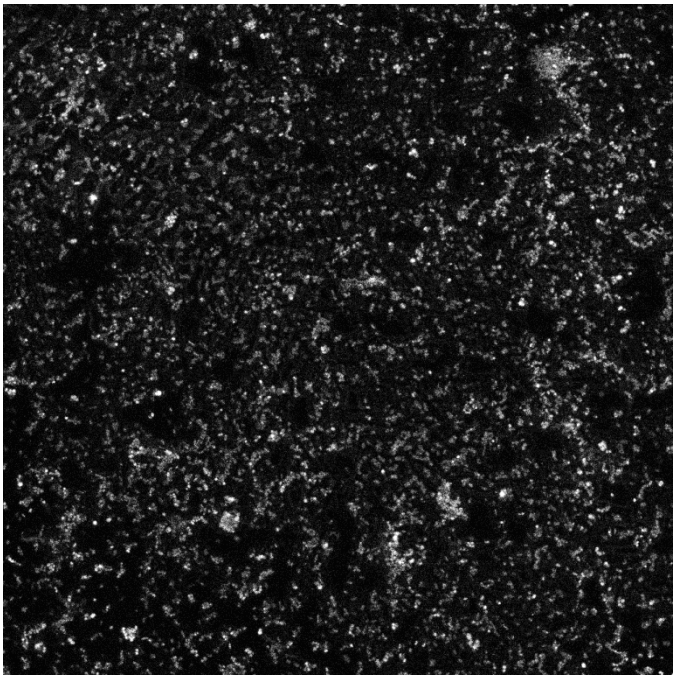

Figure 5. CLSM image of *Pantoea agglomerans* cells sloughed off of a glass bead from a column after a nanoparticle transport experiment. The image demonstrates that a biofilm was present on glass beads after transport experiments.

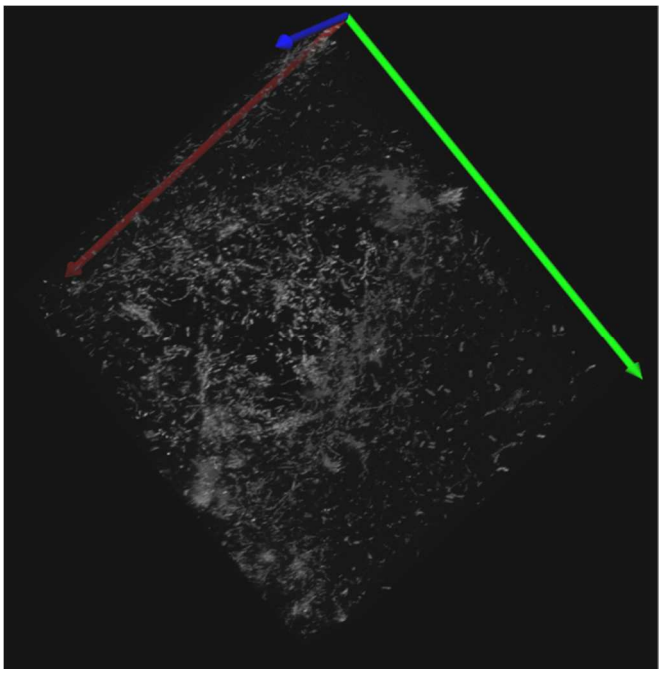

Figure 6. A three-dimensional CLSM image of *Pantoea agglomerans* biofilm adhering to a sand grain from a column after a nanoparticle transport experiment. The image confirms that a biofilm is still present in porous media after being exposed to nanoparticles; however, DAPI staining does not differentiate between live and dead cells. The green, red and blue arrows mark the x, y and z axes, respectively.

## Supporting Information

Tracer tests, evaluation of the Brus equation, determination of total organic carbon, as well as equations and parameters for attachment coefficients are available in Supporting Information.

## Acknowledgements

This research was funded by the Marie Curie Initial Training Network, IMVUL, or “Towards Improved Groundwater Vulnerability Assessment”, EU Framework 7 (Grant agreement 212298).

We would also like to thank Dr. Lorna Eades for help with ICP-OES measurements, Dr. Rosie Jones for SEM imaging, Steve Mowbray for TOC measurements, and Dr. David Kelly for CLSM imaging.

## Bibliography

Ben-Moshe, T., Dror, I., Berkowitz, B., 2010. Transport of metal oxide nanoparticles in saturated porous media. Chemosphere 81, 387-393.

Benzerara, K., Miot, J., Morin, G., Ona-Nguema, G., Skouri-Panet, F., Ferard, C., 2011. Significance, mechanisms and environmental implications of microbial biomineralization. CR Geoscience 343, 160-167.

Bergstrom, L., 1997. Hamaker constants of inorganic materials. Adv. Colloid Interface Sci. 70, 125-169.

Brock, T.D., Madigan, M.T. (eds), 1991. Biology of Microorganisms, Prentice-Hall International Inc., Englewood Cliffs, NJ.

Brus, L.E., 1984. Electron-electron and electron-hole interactions in small semiconductor crystallites: The size dependence of the lowest excited electron state. J Chem Phys 80(9), 4403-4409.

Chen, J.Y., Ko, C.H., Bhattacharjee, S., Elimelech, M., 2001. Role of spatial distribution of porous media surface charge heterogeneity in colloid transport. CSA 191, 3-15.

Chowdhury, I., Hong, Y., Honda, R.J., Walker, S.L., 2011. Mechanisms of $TiO_2$ nanoparticle transport in porous media: Role of solution chemistry, nanoparticle concentration, and flowrate. J Colloid Interf Sci 360, 548-555.

Cunningham, A.B., Sharp, R.R., Caccavo Jr., F., Gerlach, R., 2007. Effects of starvation on bacterial transport through porous media. Adv Water Resour 30, 1583-1592.

Deshpande, P.A., Shonnard, D.R., 1999. Modeling the effects of systematic variation in ionic strength on the attachment kinetics of *Pseudomonas fluorescens* UPER-1 in saturated sand columns. Wat Resour Res 35, 1619-1627.

Dror-Ehre, A., Adin, A., Markovich, G., Mamane, H., 2010. Control of biofilm formation in water using molecularly capped silver nanoparticles. Wat Res 44, 2601-2609.

Dybowska, A.D., Croteau, M., Misra, S.K., Berhanu, D., Luoma, S.N., Christian, P., O'Brien, P., Valsami-Jones, E., 2011. Synthesis of isotopically modified ZnO nanoparticles and their potential as nanotoxicity tracers. Environ Pollut 159, 266-273.

Gajjar, P., Pettee, B., Britt, D.W., Huang, W., Johnson, W.P., Anderson A.J., 2009. Antimicrobial activities of commercial nanoparticles against an environmental soil microbe, *Pseudomonas putida* KT2440. J Biol Eng 3(9).

Habimana, O., Steenkeste, K., Fontaine-Aupart, M.-P., Bellon-Fontaine, M.-N., Kulakauskas, S., Briandet, R., 2011. Diffusion of nanoparticles in biofilms is altered by bacterial cell wall hydrophobicity. Appl Environ Microbiol 77(1), 367-368.

He, F., Zhang, M., Qian, T., Zhao, D., 2009. Transport of carboxymethyl cellulose stabilized iron nanoparticles in porous media: Column experiments and modeling. J Colloid Interf Sci 334, 96-102.

Ikuma, K., Madden, A.S., Decho, A.W., Lau, B.L.T, 2014. Deposition of nanoparticles onto polysaccharide-coated surfaces: implications for nanoparticle-biofilm interactions. Environ Sci Nano 1, 117-122.

Israelachvili, J.N., 1992. Intermolecular and surface forces, p xxi, 450 p, Academic Press Ltd., London, England.

Jiang, X., Tong, M., Lu, R., Kim, H. 2012. Transport and deposition of ZnO nanoparticles in saturated porous media. CSA 401, 29-37.

Jiang, X., Wang, X., Tong, M., Kim, H., 2013. Initial transport and retention behaviours of ZnO nanoparticles in quartz sand porous media coated with *Escherichia Coli* biofilm. Environ Pollut 174, 38-49.

Joshi, N., Ngwenya, B.T., French, C.E., 2012. Enhanced resistance to nanoparticle toxicity is conferred by overproduction of extracellular polymeric substances. J Haz Mat 241-242, 363-370.

Kanel, S.R., Al-Abed, S.R., 2011. Influence of pH on the transport of nanoscale zinc oxide in saturated porous media. J Nano Res 13, 4035-4047.

Kapellos, G.E., Alexiou, T.S., Payatakes, A.C., 2007. Hierarchical simulator of biofilm growth and dynamics in granular porous media. Wat Res 30(6-7), 1648-1667.

Kapetas, L., Ngwenya, B.T., MacDonald, A.M., Elphick, S.C. (2012) Thermodynamic and kinetic controls on cotransport of *Pantoea agglomerans* cells and Zn through clean and iron oxide coated sand columns. Environ Sci Technol 46, 13193-13201.

Kosmulski, M., 2009. pH-dependent surface charging and points of zero charge. IV. Update and new approach. J Colloid Interf Sci 337, 439-448.

Kroll, A. Behra, R., Kaegi, R., Sigg, L. 2014. Extracellular polymeric substances (EPS) of freshwater biofilms stabilize and modify CeO2 and Ag nanoparticles. PLoS 9(10): e110709.

Kuhnen, F., Barmettler, K., Bhattacharjee, S., Elimelech, M., Kretzschmar, R., 2000. Transport of iron oxide colloids in packed quartz sand media: monolayer and multilayer deposition. J Colloid Interf Sci 231, 32-41.

Kurlanda-Witek, H., Ngwenya, B.T., Butler, I.B., 2014. Transport of bare and capped zinc oxide nanoparticles is dependent on porous media composition. J Contam Hydrol 162-163, 17-26.

Lerner, R.N., Lu, Q., Zeng, H., Liu, Y., 2012. The effects of biofilm on the transport of stabilized zerovalent iron nanoparticles in saturated porous media. Wat Res 46, 975-985.

Lewandowski, Z, Beyenal, H., Stookey, D., 2004. Reproducibility of biofilm processes and the meaning of steady state in biofilm reactors. Water Sci Technol 49, 359-364.

Li, M., Pokhrel, S., Jin, X., Mädler, L., Damoiseaux, R., and Hoek, E.M.V., 2011. Stability, bioavailability, and bacterial toxicity of ZnO nanoparticles in aquatic media. Environ Sci Technol 45, 755-761.

Li, Z., Hassan, A.A., Sahle-Demessie, E., Sorial, G.A., 2013. Transport of nanoparticles with dispersant through biofilm coated drinking water sand filters. Wat Res 47, 6457-6466.

Metwalli, E., Haines, D., Becker, O., Conzone, S., and Pantano, C.G., 2006. Surface modifications of mono-, di-, and tri-aminosilane treated glass substrates. J Colloid Interf Sci 298, 825-831.

Morrow, J.B., Catalina Arango, P., Holbrook, R.D., 2010. Association of quantum dot nanoparticles with *Pseudomonas aeruginosa* biofilm. J Environ Qual 39, 1934-1941.

Newman, M.D., Stotland, M., Ellis, J.I., 2009 The safety of nanosized particles in titanium oxide- and zinc oxide-based sunscreens. J Am Acad Dermatol 61(4), 685-692.

Petosa, A.R., Brennan, S.J., Rajput, F., Tufenkji, N., 2012. Transport of two metal oxide nanoparticles in saturated granular porous media: Role of water chemistry and particle coating. Wat Res 46 (4), 1273-1285.

Peulen, T.O., Wilkinson, K.J., 2011. Diffusion of nanoparticles in a biofilm. Environ. Sci. Technol. 46, 3367-3373.

Quevedo, I.R., Tufenkji, N., 2012. Mobility of functionalized quantum dots and a model polystyrene nanoparticle in saturated quartz sand and loamy sand. Environ Sci Technol 46, 4449-4457.

Ross, N., Bickerton, G., 2002. Application of biobarriers for groundwater containment at fractured bedrock sites. Remediation 12(3), 5-12.

Sato, M., Shimatani, K., Iwasaki, Y., Morito, S., Tanaka, H., Fujita, Y., Nakamura, M., 2011. New surface-modified zinc oxide nanoparticles with aminotriethylene oxide chains linked by 1,2,3-triazole ring: Preparation, and visible light-emitting and noncytotoxic properties. Appl Surf Sci 258, 786-790.

Seifert, D., Engesgaard, P., 2012. Sand box experiments with bioclogging of porous media: hydraulic conductivity reductions. J Contam Hydrol 136-137, 1-9.

Stojak, A.R., Raftery, T., Klaine, S.J., McNealy, T., 2011. Morphological responses of *Legionella pneumophila* biofilm to nanoparticle exposure. Nanotoxicology 5(4), 730-742.

Thullner, M., Schroth, M.H., Zeyer, J., Kinzelbach W., 2004. Modeling of a microbial growth experiment with bioclogging in a two-dimensional saturated porous media flow field. J Contam Hydrol 70, 1-2, 37-62.

Tong, M., Ding, J., Shen, Y., Zhu, P., 2010. Influence of biofilm on the transport of fullerene ($C_{60}$) nanoparticles in porous media. Wat Res 44, 1094-1103.

Torkzaban, S., Kim, Y., Mulvihill, M., Wan, J., Tokunaga, T.K., 2010. Transport and deposition of functionalized CdTe nanoparticles in saturated porous media. J Contam Hydrol 118, 208-217.

Tourney, J., Ngwenya, B.T., Mosselmans, F., Magennis, M., 2009. Physical and chemical effects of extracellular polymers (EPS) on Zn adsorption to *Bacillus licheniformis* S-86. J Colloid Interf Sci 337, 381-389.

Tripathi, S., Champagne, D., Tufenkji, N., 2012. Transport behavior of selected nanoparticles with different surface coatings in granular porous media coated with *Pseudomonas aeruginosa* biofilm. Environ Sci Technol 46(13), 6942-6949.

Walczak, J.J, Wang, L., Bardy, S.L., Feriancikova, L., Li, J., Xu, S., 2012. The effects of starvation on the transport of *Escherichia Coli* in saturated porous media are dependent on pH and ionic strength. Colloids and Surfaces B: Biointerfaces 90, 129-136.

Wang, D., Bradford, S.A., Harvey, R.W., Hao, X., Zhou, D., 2012. Transport of ARS-labeled hydroxyapatite nanoparticles in saturated granular media is influenced by surface charge variability even in the presence of humic acid. J Haz Mat 229-230, 170-176.

Xiao, Y., Wiesner, M.R., 2013. Transport and retention of selected engineered nanoparticles by porous media in the presence of a biofilm. Environ Sci Technol. 47, 2246-2253.

Yang, S., Ngwenya, B.T., Butler, I.B., Kurlanda, H., Elphick, S.C., 2013. Coupled interactions between metals and bacterial biofilms in porous media: implications for biofilm stability, fluid flow and metal transport. Chem Geol 337-338, 20-29.

Yao, K.M., Habibian, M.T., O'Melia, C.R., 1971. Water and waste water filtration: concepts and applications. Environ. Sci. Technol. 5(11), 1105-1112.

Zhou, D., Keller, A.A., 2010. Role of morphology in the aggregation kinetics of ZnO nanoparticles. Wat Res 44, 2948-2956.

# SUPPORTING INFORMATION

# The influence of biofilms on the mobility of bare and capped zinc oxide nanoparticles in two types of saturated porous media

H. Kurlanda-Witek[a], B.T. Ngwenya[b], I.B. Butler[b]

[a]*Mott MacDonald Polska Sp. z o.o., ul. Waliców 11, 00-851 Warsaw, Poland*

[b]*School of GeoSciences, University of Edinburgh, Kings Buildings, West Mains Rd, EH9 3JW Edinburgh, United Kingdom*

Email: hanna.kurlanda@yahoo.com

Tel. (04822) 649-4237

## 1. Tracer tests

Porosity and fluid retention time were determined by conducting bromothymol blue breakthrough curves (Cunningham et al., 1991). Two pore volumes of bromothymol blue dye, a conservative tracer, were pumped into the column at the flow rate desired for the experiment. The dye was made using a modified version devised by du Plessis and van Staden (2000) by dissolving 25 mg of bromothymol blue dye (Acros Organics) in 2.5 ml of 4% NaOH, then adding 5 ml of ethanol and deionised water to make up 250 ml. Outflow samples were collected using a fraction collector (Teledyne ISCO Retriever 500) and measured using a spectrophotometer (CamSpec M501) at 550 nm wavelength. Results show that both types of porous media possess similar flow patterns (Figure S1). Porosity calculated from column mass and flow rates was approximately 35% for sand, and 40% for 0.5 mm glass beads. For conservative tracers, one pore volume is eluted at $C/C_0 = 0.5$. Tracer tests demonstrate that one pore volume was eluted at approximately $C/C_0 = 0.7$, which may be the result of flow maldistribution, resulting in channelling between the porous media grains (Thompson and Fogler, 1997). At the flow rate of 0.46 $ml.min^{-1}$, the bromothymol blue reaches $C/C_0 = 1$ after an average of 13 minutes of tracer flow.

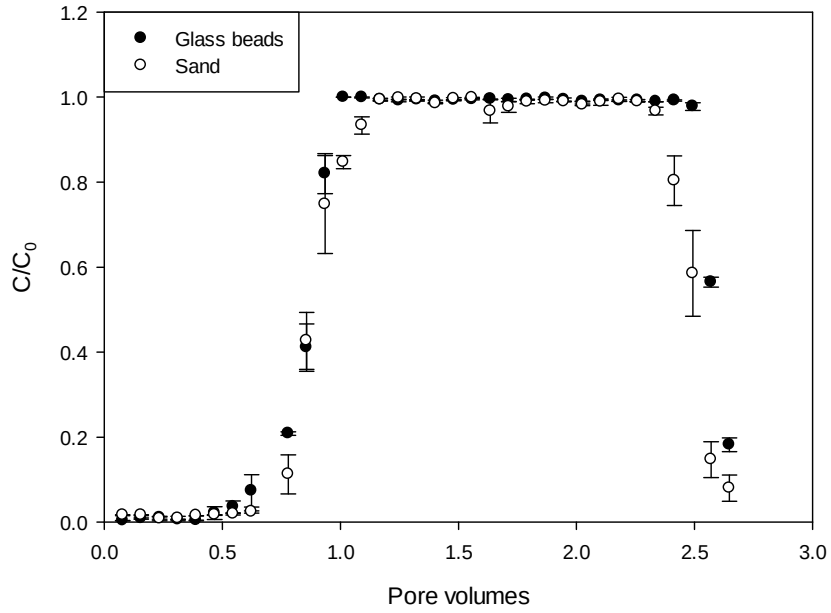


Figure S1. Bromothymol blue tracer tests show similar flow patterns for columns packed with glass beads and sand.

## 2. Measuring nanoparticle size using the Brus equation

Semiconductors, such as ZnO, possess a filled valence band, which is separated from the conduction band by a band gap. ZnO has a wide band gap (3.3 eV), and increasing nanoparticle size (i.e. aggregation), or doping nanoparticles with other metals, will result in an increase in band gap, or blue shift (Suwanboon et al., 2008). In an excited state, an electron in the valence band will be ejected onto the conduction gap, leaving an electron hole in the valence band (Murphy and Coffer, 2010). By measuring the UV-Visible absorbance of nanoparticle solutions, one can determine nanoparticle size. The highest wavelength of absorbance has to be determined in order to calculate the blue shift ($\Delta E$) (Mullaugh and Luther, 2010). The absorption of bZnO-NPs lies within the range of 360-380 nm (Ben-Moshe et al., 2010; Petosa et al., 2012; Rekha et al., 2010; Sarkar et al., 2011). The highest absorbance in our experiments was observed at 360 nm. For our instrument, and the concentration of nanoparticles used, the absorption peak of ZnO nanoparticles coated with KH550 was 375 nm. The energy of the band gap increase can be calculated from:

$$\Delta E = E_{np} - E_{bulk} = \frac{hc}{\lambda} - E_{bulk} \qquad (1)$$

where $E_{np}$ is the band gap energy of the ZnO nanoparticle,$E_{bulk}$ is the band gap energy for ZnO nanoparticles at room temperature (=3.3 eV (Berger, 1997; Sarkar et al., 2011)), $\lambda$ is the wavelength of the highest absorbance of the nanoparticle solution, $h$ is Planck's constant, and $c$ is the speed of light. $\Delta E$ is thus equal to 0.144 eV for bZnO-NPs, and 0.006 eV for cZnO-NPs. Once $\Delta E$ is known, the Brus equation can be solved for 2R, where R is the radius of the nanoparticle:

$$\Delta E = \frac{\pi^2 \hbar^2}{2R^2}\left(\frac{1}{m_e} + \frac{1}{m_h}\right) - \frac{1.8e^2}{4\pi\varepsilon_0\varepsilon R}, \hbar = \frac{h}{2\pi} \qquad (2)$$

$$\mathrm{R} = \frac{-\frac{1.8\mathrm{e}^2}{4\pi\varepsilon_0\varepsilon} + \sqrt{\left(\frac{1.8\mathrm{e}^2}{4\pi\varepsilon_0\varepsilon}\right)^2 + 4\Delta\mathrm{E}\frac{\pi^2\hbar^2}{2}\left(\frac{1}{\mathrm{m_e}} + \frac{1}{\mathrm{m_h}}\right)}}{2\Delta\mathrm{E}} \qquad (3)$$

$$\mathrm{m_e} = 0.32\ \mathrm{m_0}$$

$\mathrm{m_h} = 0.27\ \mathrm{m_0}$ (Wu et al., 2002)

where $\mathrm{m_e}$ and $\mathrm{m_h}$ are the effective masses of the electron and hole, respectively, $\mathrm{m_0}$ is the free electron mass, $\varepsilon_0$ is the vacuum permittivity, e is the electron charge, and $\varepsilon$ is the dielectric constant for ZnO (= 8.5). The resulting calculated nanoparticle radii are 3.3 nm and 7.3 nm for bZnO-NPs and cZnO-NPs, respectively, which demonstrate that the nanoparticles measured using DLS are in an aggregated state. The nominal size of nanoparticles reported by the manufacturers are based on TEM (transmission electron microscopy), which tend to aggregate nanoparticles (Baveye and Laba, 2008; Ochbelagh et al., 2012). Moreover, an independent

calibration of ZnO nanoparticle sizes by Jacobsson and Edvinsson (2011) and Jacobsson (2009), is a functional solution to the Brus equation calibrated from X-ray diffraction (XRD) data, using Scherrer's method (Scherrer, 1918):

$$E = 3.22 + \frac{0.816}{d} + \frac{294.0}{d^2} \quad \textbf{(4)}$$

where d is the nanoparticle diameter. This solution generated results for nanoparticle radii similar to ours (3.03 nm for bZnO-NPs and 8.18 nm for cZnO-NPs). Our UV-Vis measurements coincide with measurements from independent studies of the same materials (Jacobsson, 2009; Jacobsson and Edvinsson 2011). This supports our conclusion that DLS measurements represent aggregated particles.

### 3. Determination of total organic carbon (TOC)

Total Organic Carbon (TOC) was used to measure biofilm distribution in the columns. After dismantling of columns, duplicate samples of biofilm grown on porous media were stored from five column sections. TOC was measured using a modified method of Alessi et al. (2011). 100 mg of porous media sample was mixed with 20 ml of 0.5 M potassium sulphate ($K_2SO_4$) solution and sonicated in an ultrasonic bath for 30 minutes. The samples were then filtered through 0.45 µm filters (Advantec) and analysed using a Shimadzu TOC-V Analyser, with potassium hydrogen phthalate ($C_8H_5KO_4$) as standard. Samples were extracted and analysed in duplicate, and controls were made using 100 mg of clean porous media.

Due to time constraints, TOC distribution was only determined in sand columns as a proxy for biomass/biofilm distribution, and shows that there was a similar amount of biofilm in all inoculated columns (Figure S2). The area close to the column inlet possesses the highest amounts of biomass, which correlates with retention profiles of bZnO-NPs (Figure 2b) and cZnO-NPs (Figure 3b) in sand columns.

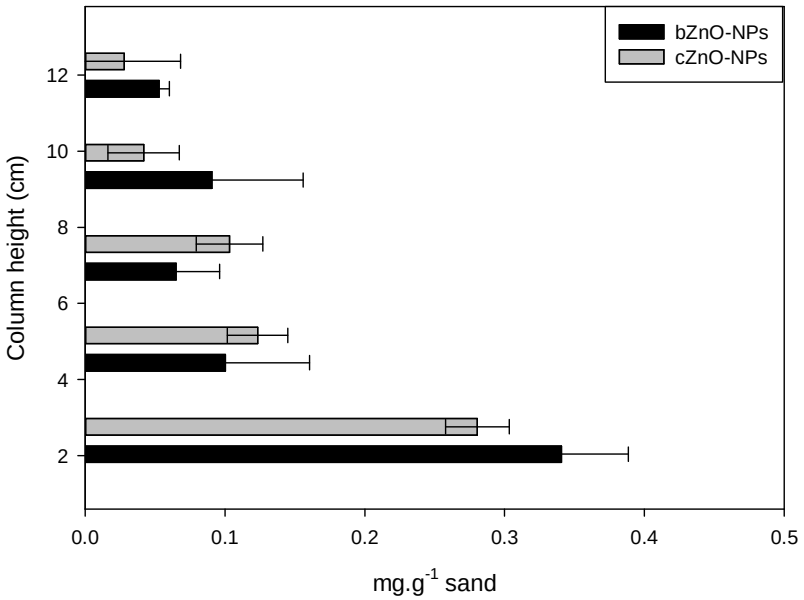


Figure S2. Total Organic Carbon of biofilm samples from sand columns after transport experiments with bZnO-NPs and cZnO-NPs. Most biofilm growth occurs at the column inlet. Error bars are standard errors of duplicate samples.

## 4. Parameters and equations for calculation of attachment efficiencies and single collector contact efficiencies

The nanoparticle attachment efficiencies (α) were calculated from:

$$\alpha = -\frac{2d_c}{3(1-f)\eta_0 L}\ln\left(\frac{C}{C_0}\right) \quad (5)$$

where $d_c$ is the diameter of the porous medium grain, $f$ is porosity of porous media, $L$ is the length of the packed column, $\eta_0$ is the single contact efficiency of the porous medium/ biofilm, and $C/C_0$ is the normalised concentration of nanoparticles flowing out of the columns. The single collector contact efficiency ($\eta_0$) of ZnO nanoparticles was calculated according to the Tufenkji-Elimelech (T-E) correlation equation (Tufenkji and Elimelech, 2004), which considers van der Waals forces, gravitational sedimentation, nanoparticle to grain size aspect ratio, porous medium porosity, fluid velocity and the Peclet number.

$$A_s = \frac{2(1-\gamma^5)}{2-3\gamma+3\gamma^5-2\gamma^6}, \gamma = (1-f)^{1/3} \quad (6)$$

$$N_R = \frac{d_p}{d_c} \quad (7)$$

$$N_{Pe} = \frac{Ud_c}{D_\infty}, D_\infty = \frac{k_B T}{3\pi\mu d_p} \quad (8)$$

$$N_{vdW} = \frac{A_{132}}{k_B T}, A_{132} = \left(\sqrt{A_{11}}-\sqrt{A_{33}}\right)\left(\sqrt{A_{22}}-\sqrt{A_{33}}\right) \quad (9)$$

$$N_A = \frac{A_{132}}{3\pi\mu d_p^2 U} \tag{10}$$

$$N_G = \frac{1}{9}\frac{d_p^2(\rho_p - \rho_f)g}{2\mu U} \tag{11}$$

$$\eta_0 = 2.4A_s^{\frac{1}{3}}N_R^{-0.081}N_{Pe}^{-0.715}N_{vdW}^{0.052} + 0.55A_sN_R^{1.675}N_A^{0.125} + \\ +0.22N_R^{-0.24}N_G^{1.11}N_{vdW}^{0.053} \tag{12}$$

Parameters used for calculation are displayed in Table S1

| Parameter | Unit | Value |
|---|---|---|
| Average nanoparticle size-bZnO ($d_p$) | m | $7.2\times10^{-8}$ |
| Average grain size-glass beads ($d_c$) | m | 0.0005 |
| Average nanoparticle size-cZnO ($d_p$) | m | $4.5\times10^{-8}$ |
| Average grain size-sand ($d_c$) | m | 0.000235 |
| Porosity – glass beads ($f$) | - | 0.4 |
| Porosity – sand ($f$) | - | 0.35 |
| Fluid velocity ($U$) | $m.s^{-1}$ | 0.0001 |
| Fluid viscosity ($\mu$) | Pa.s | 0.001 |
| Temperature | K | 298 |
| Particle density ($\sigma_p$) | $kg.m^{-3}$ | 1700 |
| Fluid density ($\sigma_f$) | $kg.m^{-3}$ | 1000 |
| Hamaker constant of ZnO ($A_{11}$) | J | $9.2\times10^{-20}$ |
| Hamaker constant of glass beads ($A_{22}$) | J | $12.1\times10^{-20}$ |
| Hamaker constant of sand ($A_{22}$) | J | $6.5\times10^{-20}$ |
| Hamaker constant of bacteria ($A_{22}$) | J | $4.8\times10^{-20}$ |
| Hamaker constant of water ($A_{33}$) | J | $3.7\times10^{-20}$ |
| Hamaker constant with biofilm ($A_{132}$) | J | $29.7\times10^{-20}$ |
| Hamaker constant without biofilm-glass beads ($A_{132}$) | J | $1.7\times10^{-20}$ |
| Hamaker constant without biofilm-sand ($A_{132}$) | J | $69.5\times10^{-20}$ |

Table S1. Parameters used for the Tufenkji-Elimelech correlation equation.

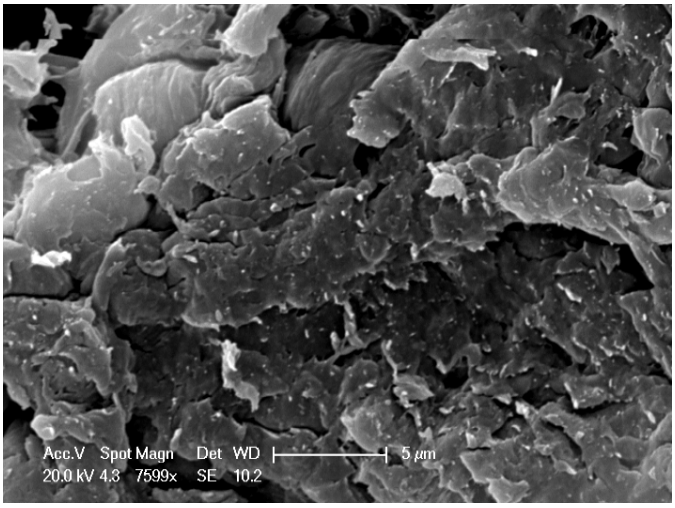


Figure S3. SEM image of ZnO nanoparticles on a sand grain from a column inlet (5 µm resolution). The nanoparticles adhering to the sand grain walls are visible as bright spots.

## 5. References

Alessi, D.S., Walsh, D.M., Fein, J.B., 2011. Uncertainties in determining microbial biomass C using the chloroform fumigation-extraction method. Chem Geol 280, 58-64.

Baveye, P., Laba M., 2008. Aggregation and toxicology of titanium dioxide nanoparticles. Environ. Health Perspect. 116(4), A152.

Ben-Moshe, T., Dror, I., Berkowitz, B., 2010. Transport of metal oxide nanoparticles in saturated porous media. Chemosphere 81, 387-393.

Berger, L.I. 1997. Semiconductor Materials, CRC Press, Boca Raton, Florida.

Cunningham, A.B., Characklis, W.G., Abedeen, F., Crawford, D., 1991. Influence of biofilm accumulation on porous media hydrodynamics. Environ Sci Technol 25, 1305-1311.

Jacobsson, T.J., 2009 Synthesis and characterisation of ZnO nanoparticles. An experimental investigation of some of their size dependent quantum effects. Master's thesis, Uppsala University.

Jacobsson, T.J., Edvinsson, T., 2011. Absorption and fluorescence spectroscopy of growing ZnO quantum dots: size and band gap correlation and evidence of mobile trap states. Inorg Chem 50, 9578-9586.

Mullaugh, K.M., Luther, G.W. III, 2010. Spectroscopic determination of the size of cadmium sulphide nanoparticles formed under environmentally relevant conditions. J Environ Monit 12, 890-897.

Murphy, C.J., Coffer, J.L., 2002. Quantum dots: a primer. Appl Spectrosc 56(1), 16A-27A.

Ochbelagh, D.R., Sohrabnezhad, S., Biroon, M.K., Golboos, N.M., 2012. Study of neutron irradiation on CoS nanoparticles grown on AlMCM-41 matrix. SAA 92, 245-249.

Petosa, A.R., Brennan, S.J., Rajput, F., Tufenkji, N., 2012. Transport of two metal oxide nanoparticles in saturated granular porous media: Role of water chemistry and particle coating. Wat Res 46 (4), 1273-1285.

Rekha, K., Nirmala, M., Nair, M.G., Anukaliani, A., 2010. Structural, optical, photocatalytic and antibacterial activity of zinc oxide and manganese doped zinc oxide nanoparticles. Physica B 405, 3180–3185.

Sarkar, D., Tikku, S., Thapar, V., Srinivasa, R.S., Khilar, K.C., 2011. Formation of zinc oxide nanoparticles of different shapes in water-in-oil microemulsion. Colloid Surf, A 381, 123-129.

Scherrer, P., 1918. Göttinger Nachrichten Gesell. 2, 98.

Suwanboon, S., Amornpitoksuk, P., Haidoux, A., Tedenac, J.C., 2008. Structural and optical properties of undoped and aluminium doped zinc oxide nanoparticles via precipitation method at low temperature. J Alloy Compd 462, 335-339.

Thompson, K.E., Fogler, H.S., 1997. Modeling flow in disordered packed beds from pore-scale fluid mechanics. AIChE 43, 1377-1389.

Tufenkji N., Elimelech. M., 2004. Correlation equation for predicting single-collector efficiency in physicochemical filtration in saturated porous media. Environ Sci Technol 38, 529-536.

Wu, H.Z., Qiu, D.J., Cai, Y.J., Xu, X.L., Chen, N.B., 2002. Optical studies of ZnO quantum dots grown on Si (0 0 1). J Cryst Growth 245, 50-55.